
Article:
Iles, L. orcid.org/0000-0003-4113-5844 (2020) Exploring the impact of iron production on forest and woodland resources : estimating fuel consumption from slag. Science and Technology of Archaeological Research.

https://doi.org/10.1080/20548923.2020.1718366

Routledge
Taylor & Francis Group

STAR: Science & Technology of Archaeological Research

ISSN: (Print) 2054-8923 (Online) Journal homepage: https://www.tandfonline.com/loi/ysta20

Exploring the impact of iron production on forest and woodland resources: estimating fuel consumption from slag

Louise Iles

To cite this article: Louise Iles (2020): Exploring the impact of iron production on forest and woodland resources: estimating fuel consumption from slag, STAR: Science & Technology of Archaeological Research, DOI: 10.1080/20548923.2020.1718366

To link to this article: https://doi.org/10.1080/20548923.2020.1718366

STAR: SCIENCE & TECHNOLOGY OF ARCHAEOLOGICAL RESEARCH
https://doi.org/10.1080/20548923.2020.1718366

Exploring the impact of iron production on forest and woodland resources: estimating fuel consumption from slag

Louise Iles

Department of Archaeology, University of Sheffield, Sheffield, UK

ABSTRACT

Reconstructing past anthropogenic influences on forest and woodland resources is an important tool to understand the development of present patterns of land use, and their long-term impacts. Past metallurgical activity undoubtedly consumed significant charcoal, exploiting forest resources for fuel at various stages of metal extraction and processing. This study aimed to quantify this fuel consumption from archaeometallurgical remains, with North Pare as a case study – a prominent centre of precolonial iron production activity in north Tanzania, and a mountainous region subject to considerable erosion processes attributed to changes in forest cover. Archaeometallurgical remains from Pare were examined with bulk chemical analysis, optical microscopy and elemental analysis to reconstruct Pare's past iron production technologies. The data was interrogated to distinguish the contribution of the fuel ash to the smelting system, with implications for our understanding of past forest degradation processes in relation to metallurgy, reducing reliance on potentially problematic analogy.

ARTICLE HISTORY
Received 3 June 2019
Accepted 13 January 2020

KEYWORDS
Iron; environment; slag; fuel ash; WD-XRF

1. Introduction

Reconstructing past anthropogenic influences on local environments and assessing their contributions to changes in those landscapes can make a valuable contribution to understanding how present patterns of land use developed, as well as anticipating the future impacts of current land use practices (Stump 2010; Finch, Marchant, and Courtney-Mustaphi 2017). Archaeology has the capacity to amalgamate cultural and environmental data over extended timescales to examine the interrelated domains of culture and nature, addressing long-term impacts of resource selection and use. Building a long-term and nuanced picture of anthropomorphic environmental change through archaeological and palaeoecological investigation is critical if the cumulative impacts of resource use are to be understood and used to inform future initiatives of land and resource use, whether for agriculture, forestry or energy.

The utilisation of forest and woodland resources is a particularly important issue. Forest cover is closely tied to processes of soil growth and erosion, as well as biodiversity – often utilised as a marker of healthy environments (e.g. Ylhäisi 2004). A range of cultural activities – including agriculture, industry and domestic activity – potentially contribute to forest depletion or degradation if poorly managed. Charcoal continues to be a significant fuel source (for cooking, heating and light) for populations in sub-Saharan Africa, South Asia, Latin America and the Caribbean (Mwampamba et al. 2013); local-scale industrial activity (such as metal smithing and ceramic production) also requires a considerable supply of charcoal as fuel. Although not widely practiced today, local, charcoal-fuelled metal production processes would have been a significant consumer of woodland resources in the past, as these technologies require the creation of long-burning and strongly reducing atmospheres within smelting furnaces (Pleiner 2000). It is thus important to ask whether past metal production technologies had a role to play in past process of forest degradation, or indeed in the maintenance of forests and woodlands through the adoption of management practices in response to increased fuel demand, and the changes in forest structure that may have ensued.

Archaeometallurgical studies that link metal production and deforestation have endured since the 1980s (see reviews in Pleiner 2000; Iles 2016). However, three core methodological problems commonly arise in some of these studies. First, there are estimates inherent within the archaeological data, such as approximations of the intensity and duration of smelting activity at a site. Second, there are estimates inherent within the environmental data, such as woodland management and procurement strategies, re-growth rates, or the effect of climate on environmental patterns. Third, there tends to be a heavy reliance on (untested and untestable) ethnographic analogy to estimate the volume or weight of charcoal needed to fuel a

CONTACT Louise Iles l.iles@sheffield.ac.uk
Supplemental data for this article can be accessed at https://doi.org/10.1080/20548923.2020.1718366

production technology. Together, these factors cast doubt on the extent to which past studies can link an intensification of metal production to forest degradation processes in a specific context.

The use of analogy (whether ethnographic or experimental) is problematic in these instances because they are in general temporally, geographically, culturally and technologically distinct from the archaeological data that they are being applied to. The range covered by the ethnographic (and experimental) record is vast, geographically and technologically, and the subsequent fuel consumption rates reported in these accounts reflect that (e.g. Humphris 2010; Haaland 1985; Charlton and Humphris 2017; van der Merwe and Avery 1987; Crew 2013; examples in Pleiner 2000). In light of this, it is prudent to ask on what basis an appropriate analogy is chosen. For unusual technologies – those utilising distinct ores or operating parameters – ethnographic analogies are even less likely to be applicable. However, this use of analogy is necessary, as there currently remains an inability to quantify the fuel required for a specific technological process in any other way.

Considering these challenges, this study sought to develop a method by which to quantify the fuel consumption of prehistoric smelting processes from archaeological remains themselves, using a case study of iron production in North Pare, northern Tanzania (Figure 1). North Pare provides a particularly pertinent setting for research to examine the relationship between iron production and landscape change. Pare is a mountainous region with montane forests on its upper reaches, mid-altitude plateaus that are dominated today by agriculture, transitioning to deciduous woodland and bushland on the lower foothills

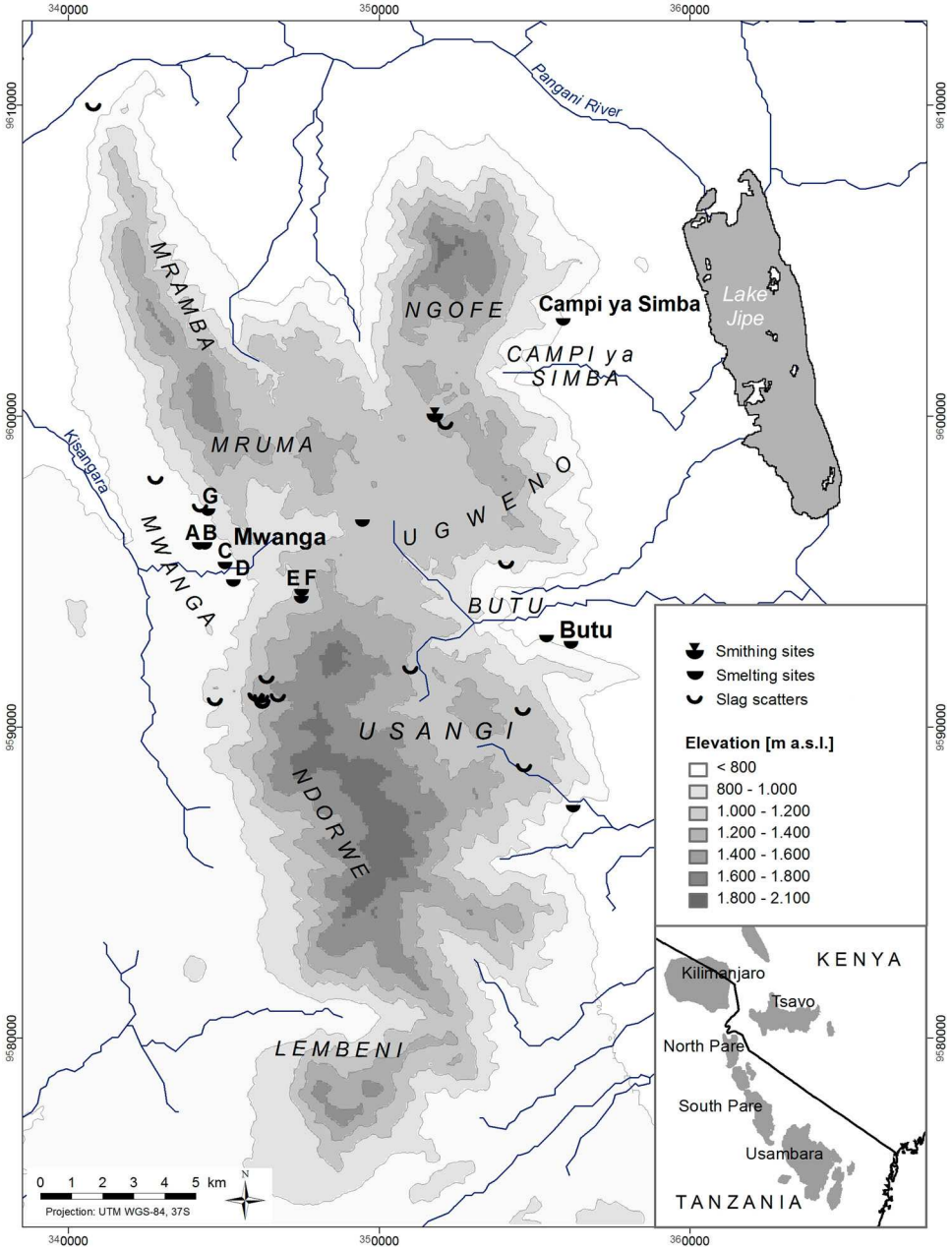

Figure 1. Map of North Pare, showing sites mentioned in the text (after Iles et al. 2018). Image courtesy of M. Heckmann.

Figure 2. (a) Typical landscape of the foothills of North Pare: the Kigonigoni hills above Butu. (b) Looking down onto the savannah plains below Mwanga G.

(Figure 2(a)) before meeting the savannah vegetation of the plains (Figure 2(b)) (Heckmann 2011, 20–21). Iron production (smelting) activity appears to have been confined to lower elevations, whereas smithing was practiced higher up the mountains (see Figure 1, Iles et al. 2018).

Pare has seen phases of significant erosion, in both precolonial and modern periods, often associated with deforestation, both historically and more recently (Mbaga-Semgalawe and Folmer 2000; Håkansson 2008; Iles et al. 2018). The history and archaeology of human-induced environmental change in Pare had not explicitly addressed iron production prior to the research presented here, although iron smelting was known to be a major precolonial industry in Pare until the early twentieth century AD (Kimambo 1996; Sheridan 2001; Kersten 1869; Baumann 1891; Meyer 1891; Kotz 1922; Holy 1957). In the neighbouring Usambara Hills, deforestation had previously been linked with iron smelting activity in the first millennium AD (Schmidt 1989). This study thus uses archaeometallurgical material from Pare to explore fuel ash consumption in past iron smelting activity through archaeological and archaeometallurgical remains. In this way, it presents an opportunity to refine our understanding of the fuel consumption of past iron smelting technologies, with implications for our understanding of past processes of landscape change, whilst reducing – though not eliminating – the current reliance on potentially unsuitable and problematic ethnographic and experimental analogy.

2. Materials and analytical methods

It is possible to deduce the inputs of a particular iron production process – the "ingredients" – from the outputs – the waste products and the remains of furnace structures (Paynter et al. 2015; Serneels and Crew 1997; Crew 2000). During a bloomery (or "solid state") smelt, iron ore is introduced into a hot, reducing atmosphere – produced by burning fuel (often charcoal) in a controlled environment. As the temperature rises above around 1200̊C, the rock minerals present in the ore begin to melt, separating from the iron oxides that remain solid throughout the process. The molten rock minerals, combined with molten elements of any ceramic, flux or fuel components amalgamate to form slag – the waste product of the process (Rostoker and Bronson 1990; Pleiner 2000). While the smelt is still underway however, the slag plays an important role in enabling the iron oxides from the ore to coalesce, as the reducing atmosphere of the furnace drives off oxygen from the system, reducing iron oxides to iron metal. The slag – as a material that chemically incorporates parts of the ore, ceramic, fuel ash and flux components of a smelting process – holds the clues to the raw materials that were utilised in a smelt. By understanding these inputs, it is possible to explore more about the local resources that were utilised by that industry.

Fortunately, waste products of iron production activity tend to be well-preserved in the archaeological record. To obtain samples of outputs from smelts, several iron smelting sites in Pare were excavated. A full description of the fieldwork strategy and the archaeology of the sites themselves is detailed in Iles et al. (2018). However, in summary, the sampling strategy focused on three smelting regions on the lower levels of the Pare Mountains: sites on the western flank of the Pare Mountains, centred behind the modern town of Mwanga; and sites on the eastern flank of the mountains, close to the villages of Butu and Campi ya Simba (Figure 1). The shape of the slag blocks were similar at all sites, though the size of the slag blocks and associated furnace remains on the eastern flank suggest that furnaces may have had a slightly smaller diameter than those to the west of the mountains. 43 samples of slag were taken from the sites designated Mwanga C and G for further analysis, and 26 slag samples were taken from Butu and Campi ya Simba. Together these provided a suitable sample by which to study the operation and ingredients of past smelting episodes in these locations.

Three core methods of analysis were used to explore the chemistry and microstructure of the sampled inorganic materials (ore, slag, ceramics). Major- and trace-element compositions of selected samples of slag (n = 69, Table 1), ore (n = 4, Table 2) and ceramic (n = 15, Table 3) were obtained by wavelength dispersive X-ray fluorescence at the Department of Geological Sciences, University of Cape Town. To compensate for any localised heterogeneity within the material, approximately 20 g of representative material were removed from each of the slag and ore samples (15 g of the ceramic samples) using a diamond-coated tile cutter blade. Material was taken from tuyère samples that showed no visible signs of vitrification, to provide a chemical composition of the ceramic with minimal contamination from the furnace charge. Any parts of the slag and ore samples that bore visible corrosion products were removed and discarded, and were not integrated into the bulk analysis. Major elements were measured on fused disks made from ignited powders (reported as wt%), while trace elements were measured on pressed powder pellets (reported as ppm). XRF analysis provides elemental concentrations that require conversion to mass percent oxides by stoichiometric calculation, based on the probable valence states of these elements. Iron oxide is reported as FeO in the slag, ceramic and ore samples, even though iron oxides are present as Fe_3O_4 in the ore samples, in order to faciliate comparison between all samples. Rubidium, uranium, lead and nickel were excluded from further analyses as on average their measured values were less than 20 ppm across the dataset as a whole, with a large proportion of concentrations below the detection limits that can be confidently measured. The raw WD-XRF data is presented in Supplementary Data 1.

The microstructures of the slag, ceramics and ore samples were also examined using optical microscopy. 31 samples of slag, 2 samples of ore and 10 samples of ceramic were mounted in epoxy resin and polished for examination in reflected light; 6 of these ceramic samples were also prepared as polished thin sections for examination in transmitted light. Elemental analysis was undertaken on a selection of these mounted samples using electron probe microanalysis (EPMA). EPMA was undertaken at two locations over the course of the research. Early analyses were conducted using a JEOL JXA 8600 electron microprobe with an Oxford Instruments EDS at the Wolfson Archaeological Science Laboratories, UCL Institute of Archaeology, London. Later analyses were conducted using a Cameca SX100 wavelength-dispersive microprobe at the Department of Space Sciences, University of Arizona. All analyses were performed at 15 kV and 20 nA. Analytical software was used to translate the measured spectra into compositional data of weight percentages, presented as oxides calculated by stoichiometry and assuming probable valence states.

Together the results of the bulk chemical analyses, optical microscopy and elemental analyses can be used to reconstruct various aspects of past iron production processes, such as operating temperatures, furnace conditions, and the materials used. To explore

Table 1. WD-XRF compositional data obtained from slag samples from sites in North Pare, normalised to 100%. "b.d." indicates that the concentration is below the detection limit of the measuring instrumentation. Iron is reported as FeO as the presence of spinels and fayalite in the microstructures indicates that a large amount of iron is in its divalent oxidation state. The mean of the raw analytical totals of the slag samples was 99.83 wt% (SD = 1.24).

	SiO_2 wt%	TiO_2 wt%	Al_2O_3 wt%	FeO wt%	MnO wt%	MgO wt%	CaO wt%	Na_2O wt%	K_2O wt%	P_2O_5 wt%	S wt%	Nb_2O_5 ppm	ZrO_2 ppm	SrO ppm	Co_3O_4 ppm	V_2O_5 ppm	BaO ppm	Cr_2O_3 ppm	ZnO ppm	CuO ppm	MoO_3 ppm	Sc_2O_3 ppm	Y_2O_5 ppm	ThO_2 ppm	Analytical total wt%
Mwanga C Slag A1	12.66	22.04	3.73	49.93	0.46	1.30	7.54	0.26	0.59	0.14	0.01	315	6598	546	54	4358	517	647	18	67	91	68	116	58	99.66
Mwanga C Slag A2	13.84	20.35	4.07	51.73	0.34	1.94	5.44	0.51	0.66	0.17	0.02	245	3542	512	72	3866	489	336	29	76	39	60	53	47	99.16
Mwanga C Slag A3	14.67	14.93	4.29	53.18	0.41	1.18	9.09	0.27	0.83	0.16	0.01	256	4709	690	74	3029	464	252	30	32	62	52	94	84	99.74
Mwanga C Slag A4	13.08	21.52	3.45	52.26	0.55	0.75	3.23	0.31	0.62	0.13	0.02	1158	36858	463	64	697	526	b.d.	70	66	571	27	105	98	99.42
Mwanga C Slag A5	14.77	23.46	4.65	47.48	0.37	1.91	4.87	0.29	0.66	0.14	0.02	292	5998	445	52	5472	557	587	22	72	82	65	73	86	99.30
Mwanga C Slag A6	11.13	17.25	3.08	58.95	0.50	0.67	4.76	0.29	0.46	0.11	0.00	820	24328	516	74	923	456	25	98	68	436	26	95	32	99.01
Mwanga C Slag A8	8.33	14.31	2.76	64.79	0.36	0.89	6.97	0.16	0.39	0.11	0.01	189	3064	589	82	4328	396	212	37	44	40	39	60	83	99.95
Mwanga C Slag A9	9.87	20.40	3.14	59.07	0.40	1.49	3.39	0.33	0.70	0.12	0.04	255	4614	374	76	4038	393	370	14	63	61	60	67	26	99.65
Mwanga C Slag A10	6.56	22.69	2.57	61.83	0.38	1.57	2.23	0.28	0.26	0.10	0.00	195	4564	207	107	7105	415	2252	35	57	66	63	95	37	99.78
Mwanga C Slag B2	23.26	16.91	4.19	48.46	0.35	0.97	3.16	0.71	0.97	0.13	0.02	271	4400	361	61	2473	478	352	76	39	53	58	90	26	99.16
Mwanga C Slag B4	13.57	19.86	3.82	56.12	0.39	0.90	2.61	0.47	0.80	0.10	0.01	273	5737	270	87	4925	490	1238	50	46	80	60	116	44	99.16
Mwanga C Slag C1	16.72	16.67	4.22	53.00	0.41	1.09	5.43	0.43	0.69	0.17	0.01	360	7696	616	74	1640	434	298	71	40	110	64	170	74	99.61
Mwanga C Slag C2	18.07	18.60	4.62	50.88	0.42	1.36	3.35	0.61	0.72	0.14	0.01	288	7127	270	65	2843	485	663	47	39	101	59	127	81	99.32
Mwanga G Slag A1	8.77	20.32	3.24	61.20	0.40	1.11	3.06	0.31	0.44	0.12	0.01	230	4384	400	80	3968	468	469	32	39	57	53	61	28	99.66
Mwanga G Slag A3	13.58	18.75	4.94	53.67	0.49	1.41	4.79	0.32	0.84	0.16	0.00	327	6068	919	64	1828	584	229	21	34	84	67	176	120	99.93
Mwanga G Slag A6	15.36	22.08	4.95	45.88	0.52	1.99	7.15	0.35	0.54	0.15	0.00	341	5992	619	59	1926	651	100	21	51	77	61	121	114	99.21
Mwanga G Slag A7	13.76	22.06	4.04	50.89	0.33	1.31	4.90	0.43	1.04	0.14	0.01	259	5179	514	66	3534	559	335	20	61	67	64	76	71	99.36
Mwanga G Slag A8	10.43	20.62	3.75	56.56	0.40	1.28	4.77	0.34	0.53	0.13	0.01	213	4326	1190	77	4461	569	939	19	46	59	56	76	19	99.84
Mwanga G Slag A9	10.21	23.49	2.50	53.67	0.28	0.70	6.86	0.25	0.81	0.22	0.02	567	5824	1171	64	1098	645	b.d.	26	43	62	47	113	294	99.01
Mwanga G Slag A11	9.55	19.91	3.95	59.20	0.51	1.28	3.38	0.35	0.57	0.12	0.01	247	5073	315	76	3945	447	1164	22	35	72	64	153	53	99.85
Mwanga G Slag A12	7.88	20.96	2.70	61.80	0.40	0.83	2.91	0.32	0.54	0.11	0.02	323	10157	345	94	3005	427	554	31	39	158	54	97	48	99.30
Mwanga G Slag A13	10.00	18.43	3.43	58.15	0.42	1.18	5.85	0.22	0.53	0.22	0.01	381	10356	747	80	2644	441	441	29	43	157	63	159	91	99.46
Mwanga G Slag A15	10.29	20.03	3.45	58.54	0.35	1.20	3.84	0.39	0.75	0.14	0.02	191	4513	363	81	3641	483	460	21	44	59	49	67	23	99.77
Mwanga G Slag B2	5.78	22.64	2.36	64.21	0.31	0.75	2.50	0.24	0.38	0.09	0.01	175	1952	316	90	3978	406	253	26	38	16	63	39	14	99.95
Mwanga G Slag B3	7.13	19.22	2.72	59.31	0.40	1.48	8.01	0.26	0.46	0.14	0.02	216	2494	562	82	3972	434	478	22	34	28	77	82	24	99.44
Mwanga G Slag B5	5.56	24.93	2.29	61.44	0.44	0.85	2.42	0.24	0.51	0.08	0.01	285	4904	232	80	5599	444	538	18	47	61	70	73	21	99.75
Mwanga G Tr. 1 (4) Slag 1	16.99	17.31	5.77	47.19	0.44	1.62	7.62	0.55	0.82	0.22	0.01	330	9067	872	70	2539	670	623	25	55	133	63	136	81	99.06
Mwanga G Slag 1	9.25	17.83	3.67	59.27	0.35	1.17	6.09	0.70	0.73	0.14	0.01	215	2820	505	87	3379	320	411	19	33	34	57	69	22	99.29
Mwanga G Slag 2	12.12	18.10	4.07	57.64	0.32	1.40	3.86	0.68	0.81	0.15	0.02	210	2904	431	90	3722	300	328	24	35	33	51	58	24	99.27
Mwanga G Slag 3	11.45	16.24	3.84	57.56	0.33	1.07	6.65	0.78	0.98	0.26	0.04	255	4033	548	83	2266	396	206	26	37	54	48	93	33	97.56
Mwanga G Slag 4	12.42	16.58	3.75	57.60	0.40	1.33	5.22	0.76	0.89	0.25	0.02	266	4035	585	78	2029	326	123	23	30	51	59	113	33	99.38
Mwanga G Slag 5	16.26	15.47	4.90	53.52	0.38	1.46	5.12	0.87	1.09	0.21	0.03	225	3131	423	79	2168	376	248	23	29	35	53	65	25	99.25
Mwanga G Slag 6	9.26	20.94	3.34	58.51	0.30	1.09	4.42	0.52	0.60	0.13	0.02	193	2753	372	86	4297	310	402	19	35	29	51	54	18	99.38
Mwanga G Slag 7	11.88	20.21	3.80	56.24	0.31	1.45	3.56	0.61	0.81	0.16	0.02	210	3578	424	87	4438	322	393	23	36	44	50	52	28	99.33
Mwanga G Slag 8	12.57	19.54	3.64	52.78	0.31	0.93	7.89	0.60	0.61	0.19	0.01	251	5083	707	67	2490	364	68	24	36	68	43	44	16	99.19
Mwanga G Slag 9	11.26	17.63	3.79	57.77	0.35	1.16	5.62	0.78	0.77	0.16	0.02	235	3252	508	75	2266	321	138	22	31	39	50	94	32	99.20
Mwanga G Slag 10	9.86	19.68	3.76	56.99	0.36	1.09	6.01	0.58	0.63	0.20	0.02	230	3076	632	81	3343	346	320	21	32	36	56	82	29	98.99
Mwanga G Slag 11	13.37	21.24	4.30	49.46	0.32	1.24	8.07	0.64	0.71	0.22	0.02	10	119	369	57	2818	416	111	23	37	0	46	22	0	99.05
Mwanga G Slag 12	15.99	16.85	5.20	52.79	0.43	1.31	4.48	0.68	1.13	0.17	0.03	309	5536	505	85	1968	333	89	38	27	78	55	170	51	99.14
Mwanga G Slag 13	11.09	18.68	4.10	56.85	0.35	1.31	4.95	0.65	0.85	0.16	0.02	262	4975	456	77	3071	329	275	18	31	66	54	115	39	99.71
Mwanga G Slag 14	15.21	16.73	4.67	53.87	0.33	1.38	5.08	0.79	0.90	0.20	0.02	229	4069	581	83	2455	376	120	21	34	52	48	77	25	100.01
Mwanga G Slag 15	7.78	16.98	3.73	63.75	0.37	1.30	3.79	0.59	0.67	0.13	0.02	224	4016	293	90	3296	258	481	22	34	55	51	81	36	99.38
Mwanga G Slag 16	10.62	17.92	4.08	59.37	0.32	1.16	4.00	0.75	0.76	0.17	0.02	219	3284	458	89	3449	300	311	21	33	40	53	74	26	99.83
Butu 1 E	12.39	19.03	4.38	57.56	0.36	1.51	3.04	0.42	0.52	0.20	0.01	137	1104	298	113	3430	426	13	91	50	11	65	79	21	99.28

(*Continued*)

Table 1. Continued.

	SiO_2 wt%	TiO_2 wt%	Al_2O_3 wt%	FeO wt%	MnO wt%	MgO wt%	CaO wt%	Na_2O wt%	K_2O wt%	P_2O_5 wt%	S wt%	Nb_2O_5 ppm	ZrO_2 ppm	SrO ppm	Co_3O_4 ppm	V_2O_5 ppm	BaO ppm	Cr_2O_3 ppm	ZnO ppm	CuO ppm	MoO_3 ppm	Sc_2O_3 ppm	Y_2O_5 ppm	ThO_2 ppm	Analytical total wt%
Butu 1 1	16.39	23.92	4.65	46.29	0.44	1.33	5.06	0.48	0.58	0.18	0.01	206	1692	579	59	3236	574	b.d.	27	48	10	96	93	30	99.62
Butu 1 3	15.43	9.10	4.91	61.18	0.44	0.79	6.57	0.31	0.68	0.25	0.03	129	378	689	80	1300	340	b.d.	28	36	0	43	22	0	99.94
Butu 2 1	8.83	23.63	3.13	57.94	0.44	1.03	3.65	0.23	0.33	0.11	0.00	154	1106	397	78	4375	508	b.d.	30	36	3	80	51	18	99.40
Butu 2 5	9.20	24.30	3.23	57.20	0.40	1.06	3.08	0.26	0.48	0.11	0.00	179	1129	357	94	4115	481	b.d.	66	38	5	77	67	23	99.08
Butu 2 A	8.06	20.66	2.99	62.86	0.42	0.93	2.90	0.25	0.37	0.12	0.01	126	915	335	83	2313	440	b.d.	48	40	0	79	47	16	99.55
Campi ya Simba Slag 1	13.69	20.53	4.52	51.30	0.45	1.48	6.11	0.46	0.43	0.19	0.03	189	3971	760	71	2510	288	b.d.	60	23	52	82	79	58	99.98
Campi ya Simba Slag 2	11.27	19.69	4.85	55.25	0.53	1.58	4.84	0.44	0.34	0.13	0.03	137	2729	660	79	6095	286	318	40	26	34	78	83	43	99.79
Campi ya Simba Slag 3	8.19	19.42	3.56	60.73	0.44	1.18	4.79	0.35	0.26	0.14	0.01	134	3425	386	83	4615	269	49	23	29	46	77	77	53	99.47
Campi ya Simba Slag 4	11.61	17.87	4.38	56.96	0.51	1.36	5.33	0.51	0.32	0.17	0.03	138	4033	580	75	4108	258	42	26	29	58	72	105	66	99.58
Campi ya Simba Slag 5	15.01	18.52	4.66	52.33	0.45	1.46	5.71	0.55	0.37	0.19	0.01	177	3013	686	88	2716	332	b.d.	48	32	38	72	97	68	99.07
Campi ya Simba Slag 6	9.89	16.89	3.48	61.67	0.49	1.07	4.87	0.44	0.31	0.11	0.01	127	2825	604	84	3457	300	b.d.	38	28	35	66	76	38	99.13
Campi ya Simba Slag 7	10.28	20.71	3.27	58.22	0.46	0.91	4.24	0.43	0.47	0.21	0.02	214	4400	543	84	1932	325	b.d.	57	29	58	80	99	79	99.30
Campi ya Simba Slag 8	15.29	19.94	4.67	47.80	0.56	1.51	8.30	0.47	0.41	0.17	0.02	172	3393	1046	63	3341	340	b.d.	27	25	42	69	83	46	99.30
Campi ya Simba Slag 9	14.40	16.80	4.17	54.82	0.46	1.16	6.22	0.45	0.44	0.22	0.03	206	5245	588	76	1404	321	b.d.	38	30	76	75	126	81	99.31
Campi ya Simba Slag 10	10.94	20.30	4.35	54.99	0.57	1.37	5.67	0.49	0.32	0.15	0.02	152	3533	681	75	3268	316	b.d.	48	28	50	72	92	50	99.07
Campi ya Simba Slag 11	10.71	16.98	4.04	60.35	0.46	1.24	4.62	0.43	0.28	0.15	0.04	131	3422	559	86	2320	241	b.d.	53	30	46	73	73	55	99.70
Campi ya Simba Slag 12	11.44	18.55	4.16	56.78	0.54	1.40	5.35	0.44	0.31	0.17	0.04	152	4373	579	81	2500	261	b.d.	30	26	62	75	111	68	99.03
Campi ya Simba Slag 13	11.17	18.94	4.36	56.97	0.44	1.44	4.82	0.43	0.39	0.16	0.02	140	2971	605	94	4216	268	108	31	32	37	71	66	49	99.40
Campi ya Simba Slag 14	14.30	18.86	4.48	51.71	0.42	1.32	6.44	0.52	0.51	0.19	0.03	255	6644	516	71	3872	315	308	31	26	95	60	100	90	99.92
Campi ya Simba Slag 15	18.10	19.58	5.13	42.56	0.52	1.57	10.32	0.66	0.48	0.18	0.05	236	4958	1382	50	1217	405	b.d.	24	21	67	84	111	76	99.21
Campi ya Simba Slag 16	8.73	17.75	3.77	61.98	0.42	1.27	4.41	0.42	0.28	0.09	0.02	136	2913	686	117	4273	270	25	30	34	45	75	75	45	99.48
Campi ya Simba Slag 17	5.63	19.47	3.62	65.33	0.45	1.34	2.53	0.40	0.17	0.08	0.02	87	2371	295	99	6344	205	b.d.	39	40	30	74	64	37	99.37
Campi ya Simba 11 Slag 1	6.72	17.94	3.07	66.50	0.41	1.28	2.64	0.20	0.16	0.09	0.00	98	2661	320	81	5870	355	68	40	56	34	76	64	42	99.92
Campi ya Simba 11 Slag 5	15.90	11.15	3.59	57.77	0.38	0.88	7.60	0.27	0.81	0.28	0.02	323	9223	797	73	2058	445	112	45	31	133	51	89	134	99.27
Campi ya Simba 11 Slag C	7.15	25.26	3.16	58.23	0.49	1.19	3.11	0.26	0.16	0.08	0.00	126	3041	454	81	4447	451	72	24	33	40	98	62	38	99.84

Table 2. WD-XRF compositional data obtained from ore samples from sites in North Pare, normalised to 100%. "b.d." indicates that the concentration is below the detection limit. Although the iron oxide in the ore was predominantly present as magnetite, iron oxide is reported as FeO to facilitate comparison with other samples. The mean of the raw analytical totals of the ore samples was 101.06 wt% (SD = 1.03).

	SiO_2 wt%	TiO_2 wt%	Al_2O_3 wt%	FeO wt%	MnO wt%	MgO wt%	CaO wt%	Na_2O wt%	K_2O wt%	P_2O_5 wt%	S wt%	Nb_2O_5 ppm	ZrO_2 Ppm	SrO ppm	Co_3O_4 ppm	V_2O_5 ppm	BaO ppm	Cr_2O_3 ppm	ZnO ppm	CuO ppm	MoO_3 ppm	Sc_2O_3 ppm	Y_2O_5 ppm	ThO_2 ppm	Analytical total wt%
Mwanga C Black sand	5.34	27.72	1.95	60.68	0.40	0.50	0.17	0.83	0.18	0.43	0.02	293	8732	9	162	3969	2612	801	594	54	133	63	93	168	99.29
Mwanga G Black sand	12.56	14.93	5.02	60.27	0.33	1.73	1.76	1.12	0.32	0.22	b.d.	329	11634	40	191	2993	214	476	560	60	183	65	201	410	99.54
Campi ya Simba Black Sand	4.02	18.88	3.12	68.81	0.33	0.78	0.52	0.80	0.08	0.12	0.02	619	14618	12	104	3385	3737	517	708	49	237	107	333	693	99.69
Butu Black sand	3.30	18.47	3.33	71.11	0.34	0.77	0.66	0.89	0.10	0.02	0.00	155	1783	15	136	4510	2466	193	668	54	21	72	38	18	99.64

Table 3. WD-XRF compositional data obtained from ceramic samples from sites in North Pare, normalised to 100%. "b.d." indicates that the concentration is below the detection limit. "Daga" is an unfired earthen building material. Values of iron in the ceramic samples are also presented as FeO to facilitate comparisons between the slag and ceramic datasets. The mean of the raw analytical totals of the ore samples was 91.64 wt% (SD = 2.25).

	SiO_2 wt%	TiO_2 wt%	Al_2O_3 wt%	FeO wt%	MnO wt%	MgO wt%	CaO wt%	Na_2O wt%	K_2O wt%	P_2O_5 wt%	S wt%	Nb_2O_5 ppm	ZrO_2 ppm	SrO ppm	Co_3O_4 ppm	V_2O_5 ppm	BaO ppm	Cr_2O_3 ppm	ZnO ppm	CuO ppm	MoO_3 ppm	Sc_2O_3 ppm	Y_2O_5 ppm	ThO_2 ppm	Analytical total wt%
Mwanga C A Tuyère	61.95	1.22	20.89	9.76	0.13	0.91	1.55	1.45	1.78	0.08	0.01	22	358	319	42	285	945	163	344	83	b.d.	41	41	5	99.13
Mwanga C B Tuyère	65.60	1.07	19.74	8.21	0.06	0.46	1.79	1.36	1.38	0.11	0.01	18	276	423	23	274	937	116	136	31	b.d.	38	30	b.d.	99.30
Mwanga C C Tuyère	65.36	1.07	19.76	8.28	0.05	0.54	1.82	1.45	1.36	0.09	0.01	18	288	392	21	262	880	105	67	36	b.d.	33	28	b.d.	99.48
Mwanga G Tr. 1 Tuyère	61.92	1.20	21.68	9.07	0.08	0.69	2.62	1.73	0.63	0.11	0.00	20	438	556	35	319	807	74	128	113	b.d.	34	24	b.d.	99.18
Mwanga G Tuyère 1	61.64	1.03	19.66	10.02	0.13	1.27	2.38	2.12	1.41	0.08	b.d.	17	273	412	40	326	1102	167	148	58	b.d.	43	51	b.d.	99.49
Mwanga G Tuyère 2	60.68	1.19	20.86	9.06	0.10	1.03	3.49	2.14	1.04	0.12	0.00	17	282	757	45	286	1292	85	107	61	b.d.	31	22	b.d.	99.18
Mwanga G Lower saddle Tuyère 1	60.38	1.11	21.37	9.34	0.14	1.12	3.51	1.87	0.71	0.12	0.00	19	323	786	48	283	1407	83	133	66	b.d.	31	30	b.d.	99.46
Mwanga G Upper saddle Tuyère 1	60.45	1.19	23.14	9.92	0.07	0.63	2.19	1.54	0.55	0.07	b.d.	16	310	506	48	309	807	88	144	51	b.d.	33	22	b.d.	99.18
Campi ya Simba Daga	67.88	0.94	17.21	6.61	0.06	0.55	1.51	1.88	2.99	0.13	b.d.	20	415	341	15	204	1057	122	65	20	b.d.	31	37	3	99.31
Campi ya Simba Furnace lining	65.53	1.53	17.69	8.47	0.08	0.50	1.36	1.55	2.88	0.11	b.d.	29	501	311	21	254	965	127	393	25	b.d.	33	56	11	99.68
Campi ya Simba Tuyère 1	63.98	1.39	18.42	9.90	0.10	0.50	2.16	1.88	1.37	0.10	b.d.	17	319	344	29	272	729	150	122	23	b.d.	45	36	b.d.	99.65
Campi ya Simba Tuyère 2	63.83	1.47	18.90	10.08	0.07	0.37	1.86	1.93	1.14	0.11	b.d.	17	333	282	24	300	870	131	203	23	b.d.	45	42	b.d.	99.01
Butu 1 Tuyère	60.26	1.38	20.87	11.27	0.09	0.50	1.97	1.64	1.53	0.23	0.00	19	298	324	34	432	1148	184	74	53	b.d.	63	42	b.d.	99.39
Butu 2 Tuyère	59.46	1.70	18.65	13.50	0.18	0.76	2.51	1.58	1.28	0.14	0.00	19	258	291	48	457	909	59	133	77	b.d.	68	54	b.d.	99.29
Butu 2 Furnace base	58.69	1.93	18.87	13.30	0.18	0.97	2.62	1.86	1.18	0.13	0.00	20	281	352	46	461	1191	78	94	76	b.d.	64	56	b.d.	99.07

more about the contributions from different material elements, principal component analysis (PCA) was used to interrogate the relationships between chemical constituents of the smelting slag samples ($n = 69$). Data were manipulated in Microsoft Excel and analysed in IBM SPSS Statistics 23. Measurements below the limit of detection (present in Y, Th, Cr) were replaced with zeros to enable PCA to take place.

A final method of analysis was used to explore the chemistry of selected samples of wood charcoal. In the absence of anthracological analyses of excavated charcoal samples, it is not possible to identify the species of wood charcoal used in past smelts at these sites. However, wood samples of tree species locally associated with charcoal production for iron production and iron working activities were instead collected from the archaeological sites of Mwanga G ("kikwata" *Senegalia mellifera* (Benth.) Siegler & Ebinger, Figure 3), Mwanga C ("mruku" *Combretum molle* R.Br ex G.Don) and Butu ("mgungu" *Faidherbia albida* (Delile) A.Chev). Information about preferred tree species was gained from local members of the extant smithing clan (see also Lyaya 2013 for discussion of charcoal species recently used in ironworking in Tanzania). Although it remains only an inference that these species may have been relevant to smelters operating across the timeframes discussed here (which could potentially date back c. 1000 years), these modern samples provided compositions of species known to be suitable for smelting, grown on soils close to the smelting sites themselves (and thus reflecting to a certain extent the elemental composition of those soils, see Jackson, Booth, and Smedley 2005). This also assumes that fuel was being sourced in the vicinity of the smelting sites, which is also not possible to confirm without anthracological analysis.

The wood samples were processed into charcoal on site using an earthmound kiln method. Subsamples were taken for acid digestion and analysis by Inductively Coupled Plasma Mass Spectrometry (ICP-MS), undertaken by Mary-Kay Amistadi at the Arizona Laboratory for Emerging Contaminants, University of Arizona using an ELAN DRC-II ICP-MS. The charcoal samples were normalised to 100% to account for unmeasured atmospheric elements (C, N, O) (Table 4). The raw ICP-MS data is presented in Supplementary Data 2.

By bringing all these strands of available evidence together, the aim was to approximate the chemical and physical operational parameters of the smelting processes being practiced in Pare and infer the raw materials that may have been used in these processes.

3. Results and discussion

Given the availability of an archaeological dataset of slag and technical ceramic samples, supplemented with ore and charcoal samples collected from the vicinity of the same archaeological sites, it was expected that the analysis of the described samples would provide an

Figure 3. Kikwata tree (*S. mellifera*) growing on the site of Mwanga G.

Table 4. ICP-MS analysis of charcoal samples from North Pare, normalised to 100%. "n.m." indicates that the concentration was not measured.

	SiO_2 wt%	TiO_2 wt%	Al_2O_3 wt%	FeO wt%	MnO wt%	MgO wt%	CaO wt%	Na_2O wt%	K_2O wt%	P_2O_5 wt%	S wt%	Nb_2O_5 ppm	ZrO_2 ppm	SrO ppm	Co_3O4 ppm	V_2O_5 ppm	BaO ppm	Cr_2O3 ppm	ZnO ppm	CuO ppm	MoO_3 ppm	Sc_2O_3 ppm	Y_2O_5 ppm	ThO_2 ppm
Mwanga C "mruku"	1.1	0.00	0.2	0.2	0.2	11.9	25.8	0.8	45.2	13.1	n.m.	n.m.	11	8760	2	13	1328	28	475	655	34	n.m.	8	n.m.
Mwanga G "kikwata"	1.3	0.01	0.9	0.3	0.1	11.0	34.7	0.7	39.0	9.3	n.m.	n.m.	18	20634	37	13	3655	34	544	362	56	n.m.	2	n.m.
Butu "mlungu"	1.3	0.01	0.6	0.3	0.2	12.0	37.8	0.7	30.4	14.3	n.m.	n.m.	7	15610	2	11	4670	11	1008	567	33	n.m.	9	n.m.

opportunity to move towards quantification of the fuel ash consumption of a smelting process, as previously discussed. To this end, the data was interrogated with the aim of:

- identifying the signature of the chemical contribution to the slag from the ore, technical ceramics and any potential fluxes,
- deducing the signature of the contribution from the fuel ash,
- estimating the relative contribution of fuel ash to the slag melts of past smelts.

Each stage of this investigative process is discussed in turn below.

3.1. Inferring chemical contributions to the slag melt

The ore – specifically the unwanted gangue minerals associated with the iron oxides of an ore – is the major contributor to slag chemistry in bloomery smelting systems. A not-insignificant proportion of iron oxide is also lost to the slag during a smelting episode to produce slag of a sufficiently low melting temperature and viscosity to separate cleanly and easily from the forming bloom. The bulk chemistry of the Pare slag was immediately notable for its exceptionally high titania content, ranging up to 25 wt% with an average of 19 wt% (Table 1). The high titania was reflected in the microstructure of these samples, which were dominated by pinkish spinels of ulvite (Fe_2TiO_4) (Figure 4). Ti-rich ilmentite was also present in residual magnetite grains trapped in some of the slag samples (Figure 5). Together, these chemical and microstructural data provide a clear link between the ores used in past smelting episodes and the magnetite-ilmenite black sands that are present in the riverbeds across the North Pare foothills. Samples of these black sands, collecting during the fieldwork, were also examined chemically and microstructurally (Table 2, Figures 6 and 7). From these analyses, it is possible to ascertain that the primary constituents of the ore sands are TiO_2 (approx. 15–28 wt%), FeO (average 65 wt%) and SiO_2 (average 6 wt%). Of the trace elements measured, zirconia stands out as both high and variable, measuring almost 2000 ppm at Butu and 15000 ppm at Campi y Simba (while measuring c. 10,000 ppm at the Mwanga sites).

Often it is difficult if not impossible to identify the exact ore used in a past smelting process. The signature of the Pare ore is unusual and distinctive, and clearly indicated in the titania-rich chemistry and ulvite-dominated microstructure of the North Pare slag samples. This is a relatively rare example of a smelting technology on the African continent exploiting ilmenite-rich magnetite ore sand (Ige and Rehren 2003;

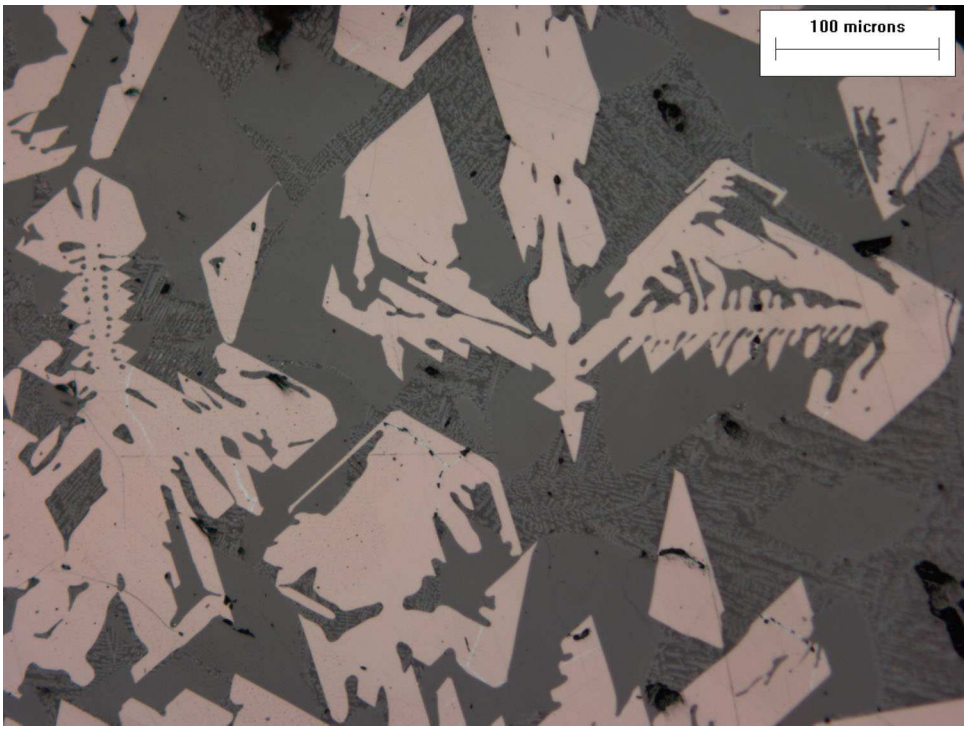

Figure 4. Photomicrograph of a slag sample from Campi ya Simba. Pinkish ulvöspinels (pink) in a fayalitic/kirschsteinitic groundmass (grey). Porosity in the sample appears black.

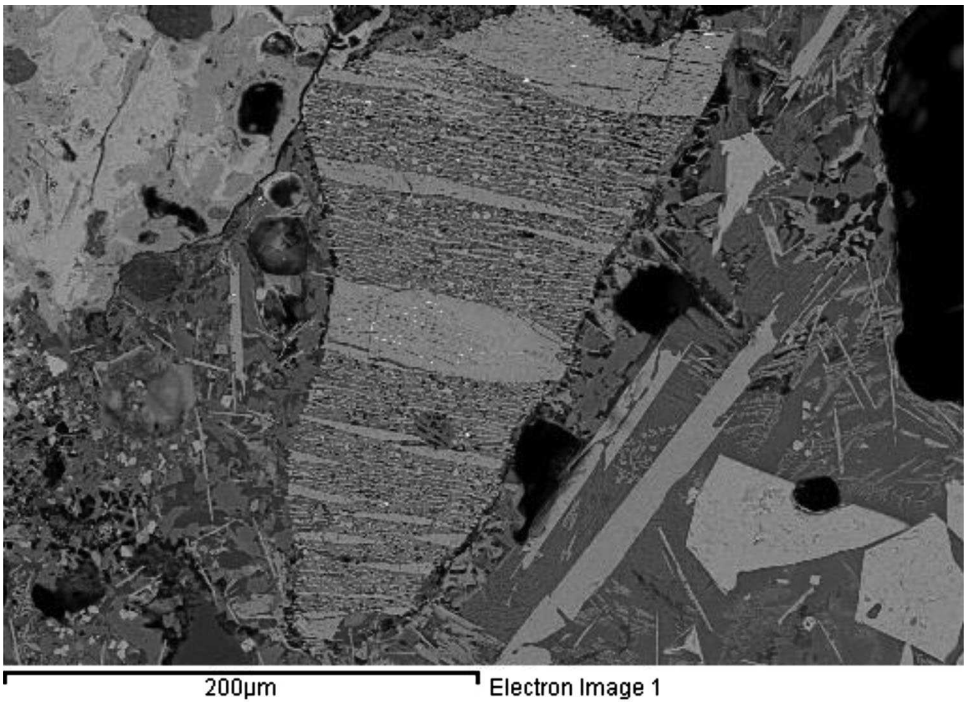

Figure 5. Back-scattered electron image of a magnetite-ilmenite grain entrapped near the surface of a slag sample from Mwanga C.

Ige 2013; Iles and Martinón-Torres 2009; Killick and Miller 2014; Mapunda 2003). As such, in this instance, it has been possible to confidently demonstrate the particular ore that was used, and also ascertain that ore samples from across North Pare are compositionally similar.

The use of a flux – a material added to a smelt to aid the separation of slag from bloom – is a potentially significant contributor to slag chemistry that must be considered. The low gangue content of many magnetite ores is generally associated with the use of quartzitic flux to form slag (e.g. Killick and Miller 2014). However, although the ore in Pare is magnetitic, because it is obtained from river sands it is mixed naturally with other river sands derived from the quartz-feldspar granulites of the slopes of the Pare Mountains (Bagnall 1960).

Figure 6. Sample of black sand from Mwanga C, North Pare.

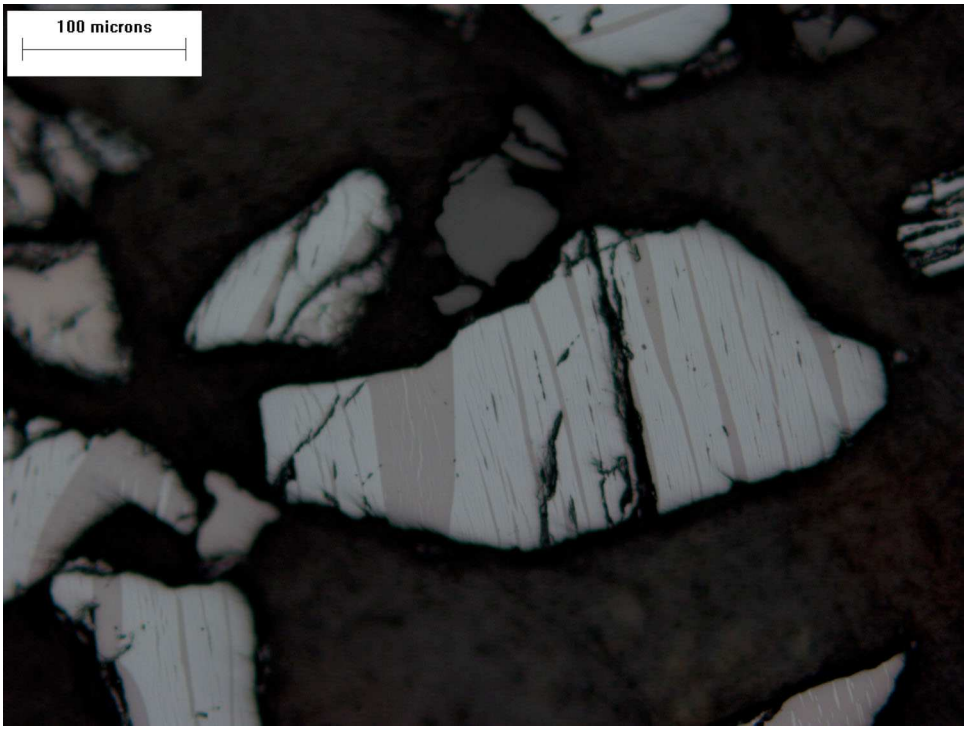

Figure 7. Photomicrograph of black sand sample from Mwanga G, illustrating the ilmenite-magnetite banded grains.

The ratio between quartzitic and magnetitic components will vary depending on the winnowing and washing processes applied to the collected ore sands, as well as seasonal changes in water courses and river levels. This will ultimately impact on the amount of silica present in the ore, but also any associated minerals.

The ore bearing sands collected for this research were initially washed with water in a pan to facilitate the removal of the quartz component, then run over once with a magnet to further improve the magnetite concentration. This resulted in silica values between 3 and 13 wt% (Table 2). The FeO–SiO_2 phase diagram indicates that FeO fluxed with < 15 mass% SiO_2 results in only a minimal reduction in the theoretical liquidus temperature (from ~1377 to ~1300°C). This is high for a bellows-powered furnace, and for a free-flowing slag the temperature would have had to be maintained at approximately 100°C above that (Killick and Miller 2014). In practice, the liquidus temperature would be lower due to the added fluxing qualities of CaO and additional SiO_2 from ceramic and fuel ash contributions to the melt. Indeed, plotting the slag samples in a FeO–TiO_2–SiO_2-5%Al_2O_3 phase diagram (Itaya et al. 2014) indicates minimum liquidus temperatures slightly lower than those estimated by the FeO–TiO_2–SiO_2 ternary diagram (Verein Deutscher Eisenhüttenleute 1995), yet still predominantly in the range of 1250–1350°C (Figure 8). Considering the agreement between these temperature ranges, and in the light of the similarity between the silica to alumina ratios in the ceramic and slag samples (both 3:1), it is unlikely that an additional silica-rich flux was added to these Pare smelts.

An initial PCA of the entire WD-XRF database (including all slag, ore, fuel and ceramic samples, n = 91) describes the compositional ratios associated with each of the smelt ingredients, and indicates that the slag is – as would be expected – heavily influenced by the composition of the sampled ores. PCA biplots of the first three principal components reveal patterns that are indicative of the chemical contributions from the different smelt ingredients. Three groups are distinguished in bi-plots of PC1 (40% of variance explained) against PCs 2 (24%) and 3 (12%) (Figures 9 and 10). SiO_2, $Al2O_3$ and NaO_2 – which share statistically significant, strongly positive correlations – are compounds associated with entering the slag melt from the ceramics. This ceramic-dominated chemical group negatively correlates along PC2 with compounds that describe the fuel samples: MgO, CaO, K_2O, P_2O_5, SrO and CuO. Finally, this fuel-related group is separated along PC1 from the ore-related compounds, predominantly the oxides of Fe, Ti, Mn, Co, V and to a lesser extent Sc – a group which also shares statistically significant and strongly positive internal correlations.

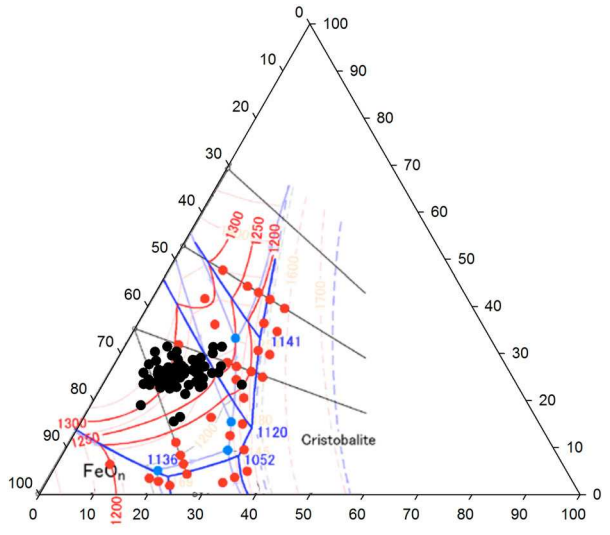

Figure 8. Ternary phase diagram showing all slag samples from North Pare (marked with black circles), in the FeO–TiO_2–SiO_2-5%Al_2O_3 system (after Itaya et al. 2014).

PCA of the archaeological samples was then used to explore the contribution of parent materials to the furnace melt (Figures 11 and 12), using data from only those materials that are commonly obtained from an archaeological excavation (tuyères and slag). The strong correlations present in the analyses of the full dataset (Figures 9 and 10) were diminished, yet were still distinguishable. The ceramic and non-ceramic contributions separated predominantly along PC1, with very high correlations between SiO_2, Al_2O_3 and Na_2O (>0.9), strongly negatively correlated with compounds associated with the ore – FeO, TiO_2 (–0.9). The ore and fuel contributions separated along PC3 (and less clearly along PC2), with strong positive correlations between SrO and CaO (0.6) and to a lesser extent P_2O_5 (0.4–0.6).

This general pattern is replicated when considering the slag dataset alone. The compositions of the slag samples are overall relatively consistent, however there is some – though minimal – chemical variation; although generally consistent in terms of materials, the smelting technologies used across the Pare Mountains incorporated some natural variation in terms of inputs and operating parameters as would be expected. Again, correlations within the compositional dataset can be used to infer the parent material that each variable relates to. The compositional similarity of the slag samples (as compared to the full dataset) makes these correlations weaker, and less easy to define. However, very strongly positive, statistically significant correlations remain between silica and alumina (ceramic contribution, 0.8), and between lime and strontium oxide (fuel contribution, 0.70).

3.2. Estimating fuel:ore ratios

Estimated materials (or mass) balances undertaken on compositional data derived from experimental smelts have been able to approximate the inputs and outputs of specific smelting systems from slag analyses (e.g. Crew 2000; Serneels and Crew 1997). However, it is notoriously challenging to achieve a stable mass balance with typical archaeological datasets, which are inevitably incomplete, in particular often lacking

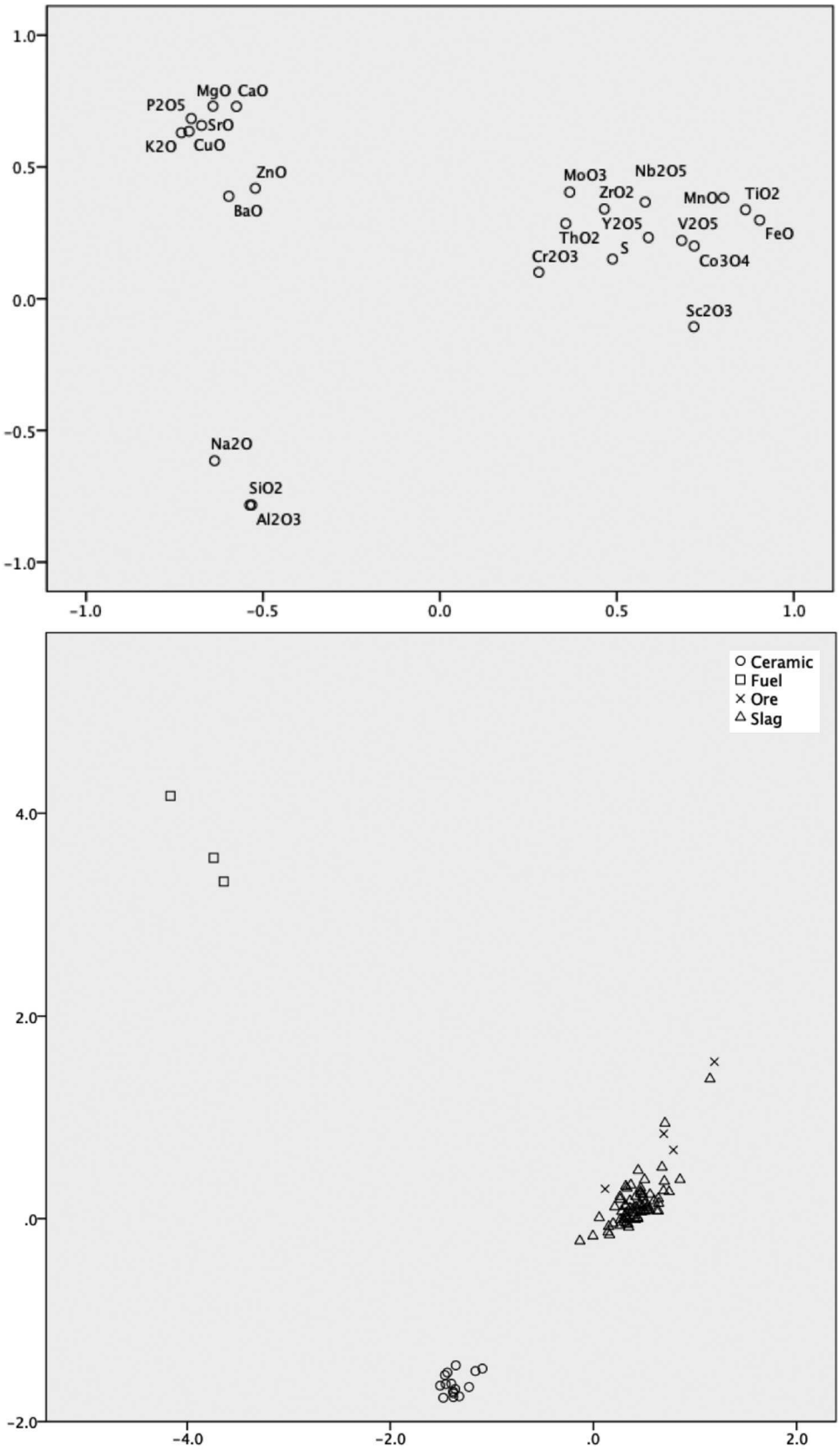

Figure 9. Bi-plots of all analysed samples (bottom) in principle component space (top); PC1 (*x*-axis) vs PC2 (*y*-axis).

examples of the ore that was used in past smelts, and examples of charcoal that would have been used in past smelts, but which had not been chemically altered in the smelt. The data from Pare combines archaeological (slag, ceramics) and modern (ore, charcoal) data, which inevitably makes any calculations more difficult.

The ore samples are modern collections, and may not reflect the compositions of ores used in the past at these sites. It is certainly likely that the past Pare smelters may have collected and processed the black sands differently in order to obtain a cleaner ore with a higher proportion of iron oxide minerals. The charcoal data of

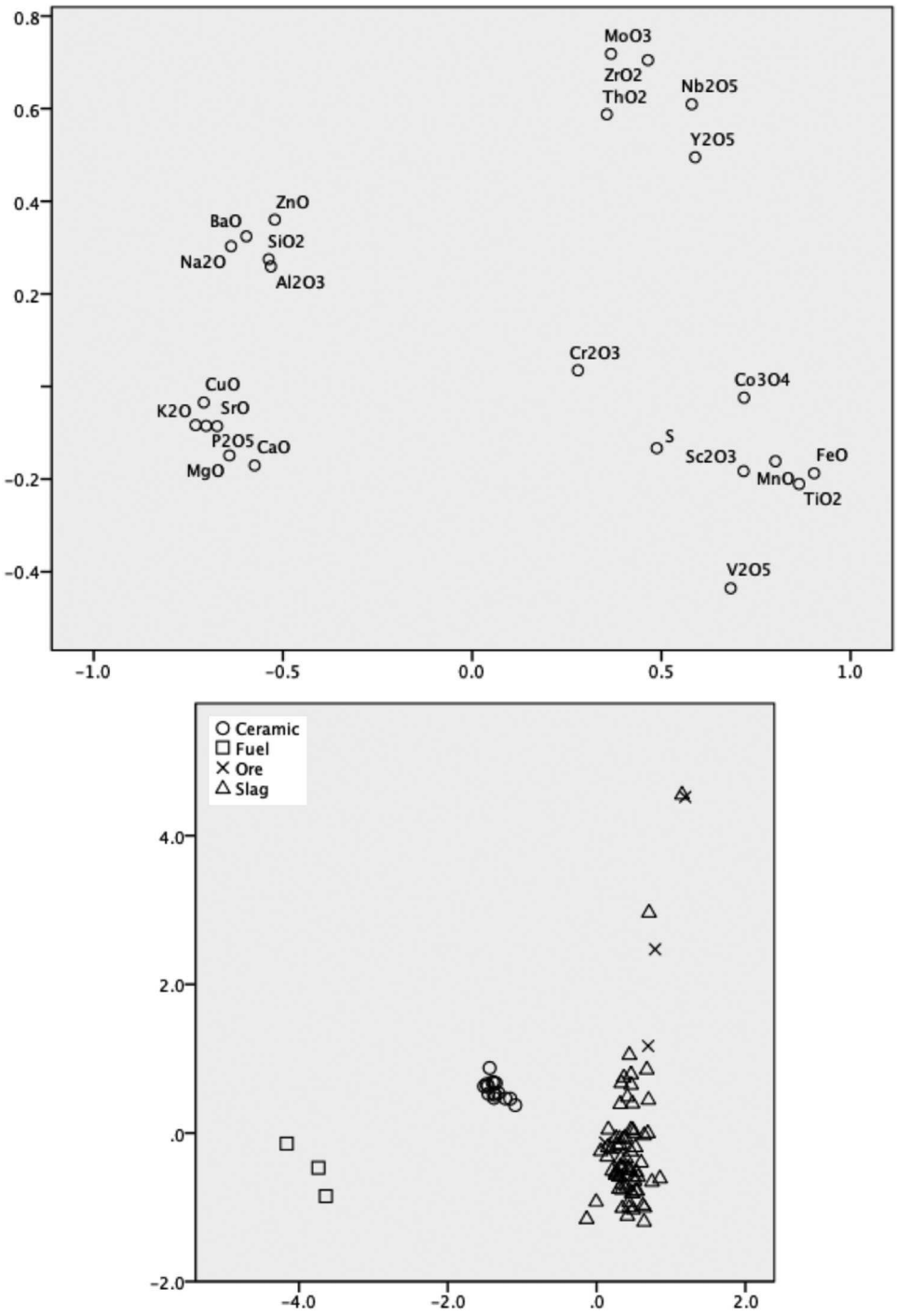

Figure 10. Bi-plots of all analysed samples (bottom) in principle component space (top); PC1 (*x*-axis) vs PC3 (*y*-axis).

the current research also builds from several inferences: the species were selected due to ethnographic information associated with them, and prepared as charcoal on a very small scale by researchers inexperienced in making charcoal. The wood the charcoal was made from, however, was collected from the iron production sites themselves, and thus those trees would have been more likely to have a similar chemical signature to those obtained from there in the past, influenced by the subsoil (and thus soil) they grew on.

Also potentially relevant here in terms of the archaeological evidence is the presence of large white shells of African land snails, especially common at the smelting sites on the eastern flank of the Pare mountains. Although the use of a quartzitic flux – as previously discussed – is deemed unlikely, it is feasible that crushed snail shells may have been added to the smelts as an additional source of lime (such shells are likely to have compositions of around 50 wt% CaO, Yao et al. 2014): this would have had a fluxing affect. It is, however, not possible to verify this hypothesis – no crushed shells were found at the sites, only whole shells, and no shell was identified that was adhering to slag, either macroscopically or microscopically.

As such, it was unfortunately not possible to create a convincing mass balance from this data, not least

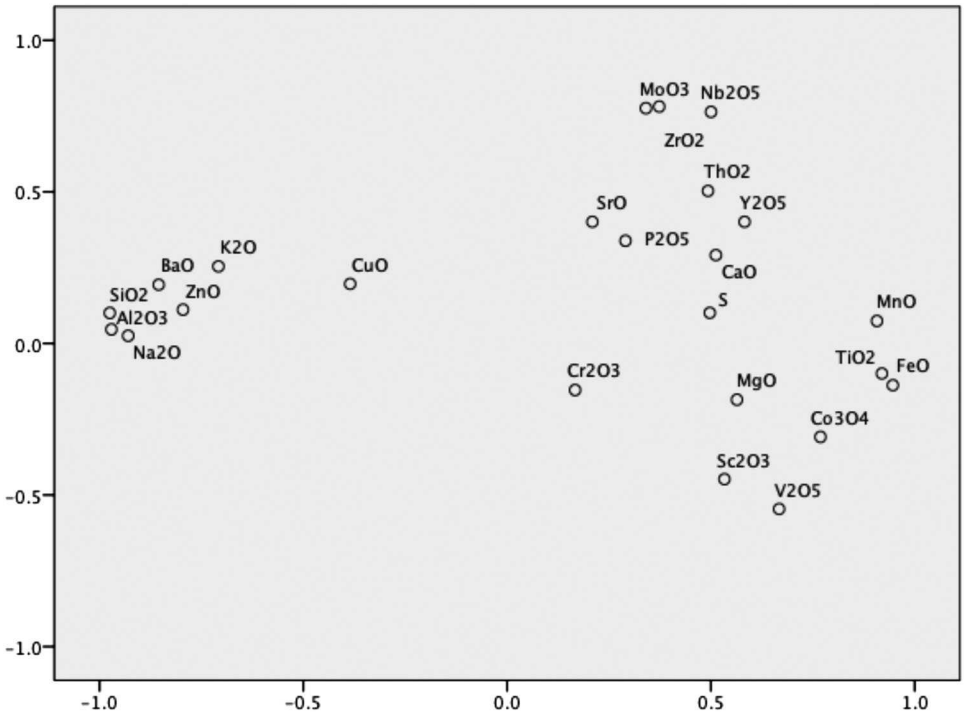

Figure 11. PCA of archaeological samples (slag and tuyère) (PC1 vs PC2). PC1 (*x*-axis) explains 45% of the variance; PC2 (*y*-axis) explains 14%.

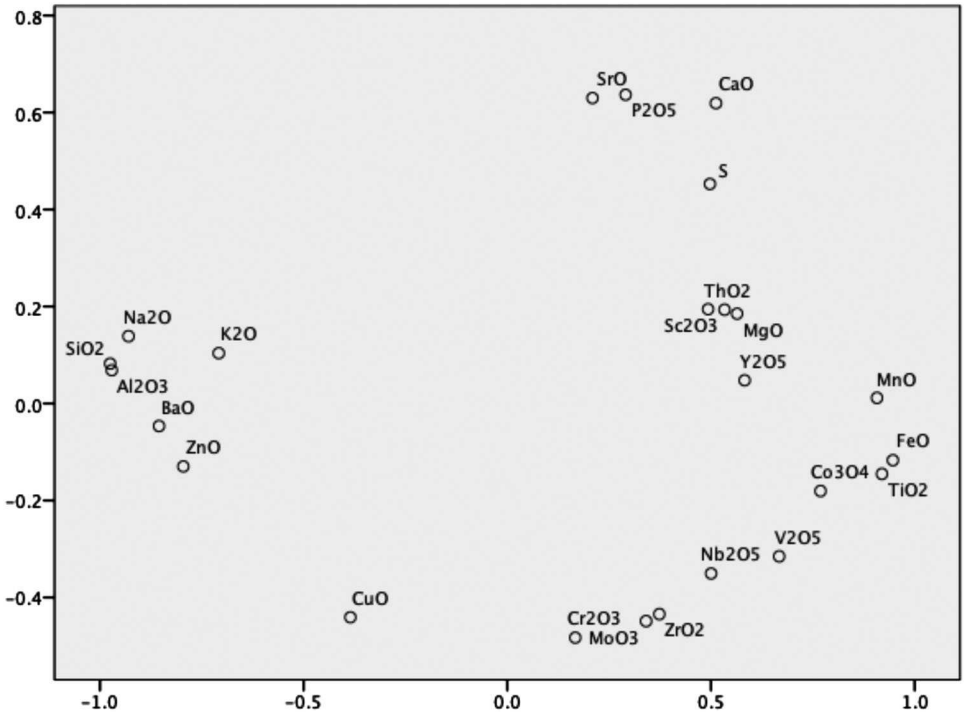

Figure 12. PCA of archaeological samples (slag and tuyère) (PC1 vs PC3). PC1 (*x*-axis) explains 45% of the variance; PC3 (*y*-axis) explains 11%.

because the iron content of the ores was roughly comparable to the iron content of the slag samples. Instead, in order to develop a general idea of the ratio between ore inputs and fuel ash inputs, a selected compound associated with the ore (MnO) was compared with a selected compound associated with the fuel ash (SrO). These compounds were selected on the basis of having the weakest correlations with those from the other categories of ingredients (ceramic, fuel ash, ore) as expressed in the slag PCA (volatile elements such as zinc were deemed unsuitable for this, as were elements which were not measured in the fuel ash

Table 5. Calculations to estimate relationship between fuel ash and ore contributions to slag, through MnO and SrO ratios.

Mwanga G	Ore	Fuel ash	97.5% ore	2.5% fuel ash	Modelled total	Mwanga G slag (ave)
MnO (wt%)	0.334	0.063	0.326	0.002	0.328	0.374
SrO (wt%)	0.004	2.063	0.004	0.052	0.055	0.055
Mwanga C	Ore	Fuel ash	95% ore	5% fuel ash	Modelled total	Mwanga C slag (ave)
MnO (wt%)	0.402	0.151	0.382	0.008	0.389	0.411
SrO (wt%)	0.001	0.876	0.001	0.044	0.045	0.045
Butu	Ore	Fuel ash	97.5% ore	2.5% fuel ash	Modelled total	Butu slag (ave)
MnO (wt%)	0.338	0.174	0.330	0.004	0.334	0.415
SrO (wt%)	0.001	1.561	0.001	0.039	0.040	0.044
Campi ya Simba	Ore	Fuel ash (Butu)	96% ore	4% fuel ash	Modelled total	Campi ya Simba slag (ave)
MnO (wt%)	0.328	0.174	0.315	0.007	0.322	0.472
SrO (wt%)	0.001	1.561	0.001	0.062	0.064	0.064

samples (scandium), or where additional contributions, such as a shell flux, may have skewed the data, e.g. CaO).

These calculations suggest that the fuel ash component of the slag in relation to the ore gangue was in the range of 1:20–1:40 fuel ash:ore gangue (Table 5). On the basis of these estimations, each kilogram of slag at Mwanga G contained an estimated 25 g of fuel ash; at Mwanga C, 50 g. This, however, needs a further step to convert this into an estimation of the relative volume of charcoal.

The analytical total of measured components of the charcoal samples (not including measurements of moisture content, atmospheric elements (C, O, N), or volatile elements – though the samples of charcoal were not ashed prior to analysis in order to not lose volatile elements) totalled between 0.7 and 1.2 wt% (Table 4). This fits within typical boundaries for charcoal compositions (which tend to have between 1 and 5% moisture content, 0.5–5% ash content, 5–40% volatile matter and 50–90% carbon content). At Butu (and by extension, Campi ya Simba), 2.5 kg of measured fuel oxides would thus be the equivalent of 244 kg prepared charcoal. At Mwanga G, 2.5 kg of measured fuel oxides would thus be equivalent of 274 kg prepared charcoal. Each kilogram of slag at Mwanga G would have been the product of the burning of 2.74 kg charcoal.

Extrapolating from the Mwanga G data (Table 5) suggests that 274 kg of charcoal would be needed to process 97.5 kg of ore, a ratio of approximately 1:3 (ore:charcoal) by weight. To give a rough idea of how this might convert to volume, conversions to m^3 were estimated. With estimates of 1 kg of charcoal equivalent to c. 0.003 m^3 (FAO 1983: Annex IIIb, 2.1) and 1 kg magnetite-ilmenite sand equivalent to c. 0.0002 m^3 (specific gravity of magnetite = 5.2; specific gravity of quartz sand = 2.7), a ratio of ore to charcoal of approximately 1:42 by volume is determined.

These estimated ratios seem reasonable when compared with data derived from ethnographic and experimental work. An iron smelting reconstruction in Rwanda saw 228 kg charcoal used to smelt 40 kg ore (a mix of five different ores, including magnetite sands and massive haematite) – a ratio of 1:5.7 (ore:charcoal) (Humphris 2010, 42). Reconstruction of Mafa smelting in Cameroon, using magnetite sands, used 82.3 kg charcoal to smelt 18 kg of ore – a ratio of 1:4.6 (ore:charcoal) (David et al. 1989). At the extreme end of observations of charcoal consumption, natural draught furnaces in Malawi (Chulu and Phoka smelts) saw fuel consumption of 1000–1450 kg charcoal to process 55–75 kg of low-grade lateritic iron ore, ratios of ore to fuel of 1:19 (Chulu) and 1:18 (Phoka) by weight (van der Merwe and Avery 1987) – a much higher rate of fuel consumption.

3.3 Applying this data at Mwanga G

The intention of the calculations reported here was not to examine how much iron was produced from these smelts. Instead, this study aimed to quantify the fuel ash component of a bloomery smelting system, which could be fed into questions assessing the impact of iron production on local forest resources. Thus, what is more valuable here is to estimate the slag to fuel ratio in order to estimate the total amount of fuel needed at an individual site. The new data was explored using the site of Mwanga G as a working example. Although production intensity, wood take-off, species selection and regeneration capacity are important factors in estimating forest impact, it was not possible to take all of these additional factors into account in the course of this research.

To explore the intensity of production activity at the site of Mwanga G, the volume of slag remains were estimated using the guidance of a magnetometry survey (Figure 13), which was combined with chronological data (Table 6). The chronological aspect of the study was fairly limited in the precision of the data it produced, namely because there were few radiocarbon dates due to the lack of charcoal remains recovered from secure excavated contexts, and because of the broad calibration ranges associated with the dates that were obtained.

The smelting activity at Mwanga G was contained within a flat area on the saddle of a foothill; it was surrounding by steep slopes on all sides, which meant that smelting activity could only have taken place in a limited area. The source of ore for the site was likely to be

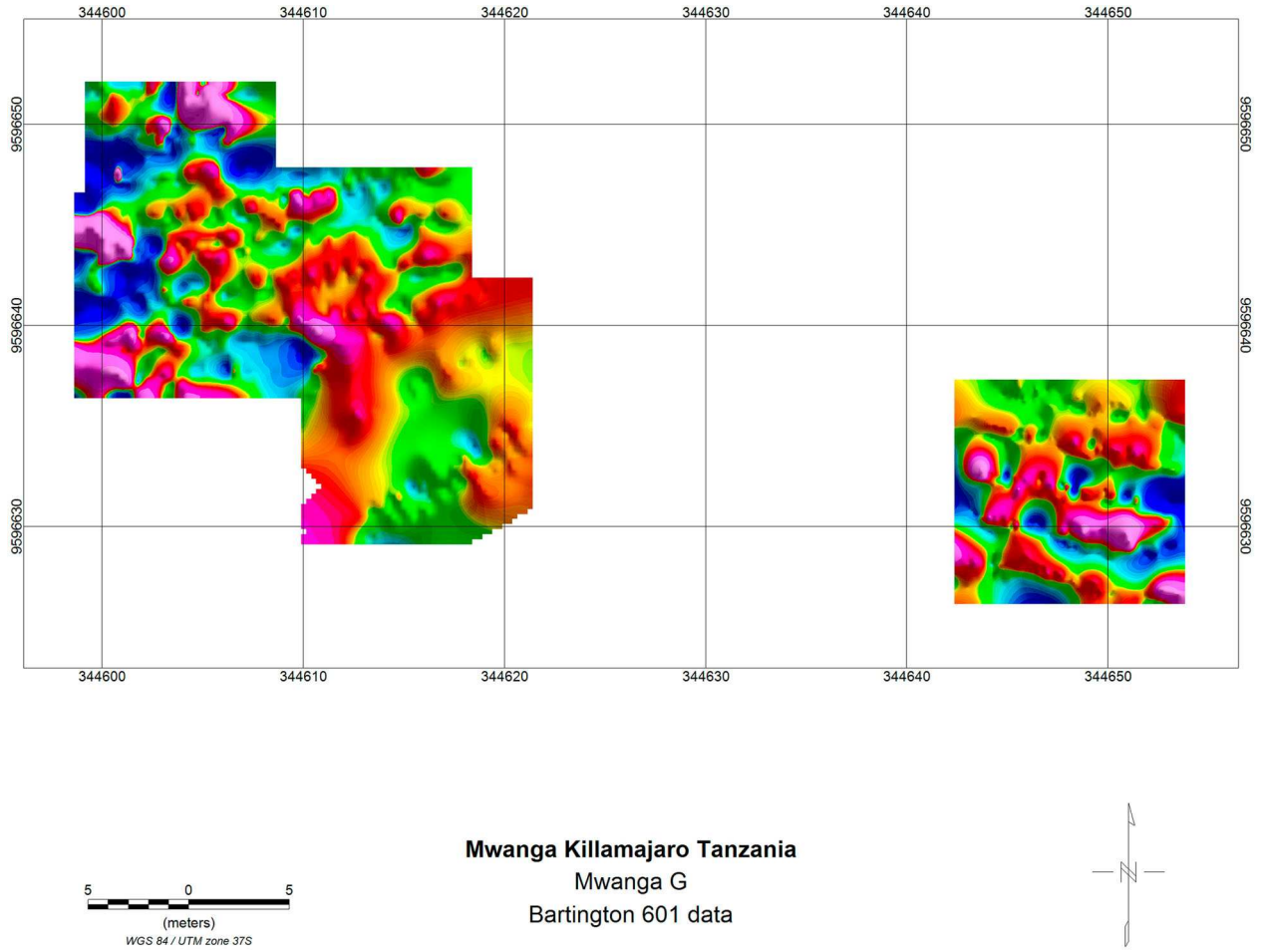

Figure 13. Shaded relief map of the magnetic gradient results for Mwanga G. Image courtesy of G. Heath.

Table 6. Radiocarbon dates obtained from iron production sites in North Pare, calibrated using OxCal 4.2, to 95.4% probability (Bronk Ramsey 2009; Hogg et al. 2013; Reimer et al. 2013).

Site	Feature/deposit	Lab code	C14 age	Calibrated date (SHCal 13)	Calibrated date (IntCal 13)
Mwanga A	Furnace fill	LTL5138A	862 ± 40 BP	1157–1278 AD	1044–1260 AD
Mwanga C	No context information	N-649	1020 ± 110 BP	791–1275 AD	769–1244 AD
	Furnace fill	LTL5140A	560 ± 50 BP	1316–1459 AD	1298–1436 AD
Mwanga G	Tuyère pile	LTL5139A	366 ± 45 BP	1461–1643 AD	1447–1636 AD
	Slag-rich deposit	AA103978	873 ± 36 BP	1155–1274 AD	1042–1248 AD
Campi ya Simba	Slag-rich deposit	AA103979	900 ± 36 BP	1048–1270 AD	1036–1213 AD
	Slag-rich deposit	AA103980	927 ± 36 BP	1045–1223 AD	1024–1185 AD
	Slag-rich deposit	AA103981	945 ± 36 BP	1040–1213 AD	1020–1165 AD
	Slag-rich deposit	AA103982	900 ± 36 BP	1048–1270 AD	1036–1213 AD

derived from the stream bed running next to the site, which carried black sands. Magnetic gradient datasets were collected using a Bartington 601 fluxgate gradiometer at a sampling density of 8 measurements/m^2 on five 10 m × 10 m grids with some overlap (Heath 2015). In an ideal scenario, geophysical survey should cover the site of interest as well as adjacent areas to improve data interpretation. This was restricted somewhat at Mwanga G by the abrupt and steep incline of the hillsides and the frequent vegetation at the site. Instead, where it was not possible to gather gridded data, the Bartington 601 was used to survey on reconnaissance mode. Significant anomalies identified both through an initial analysis of the gridded data and the reconnaissance survey data were explored through surface ground-truthing (e.g. identifying exposed bedrock with magnetic magnetite seams); anomalies not explained in this way were investigated with 1 × 1 m test-pit excavations. Unfortunately, no archaeological features such as furnaces were found using this methodology. However, the test-pits provided a valuable sample of the distribution of buried slag and tuyère remains, and the limited thickness of the archaeological deposits remaining on the hilltop (Table 7).

Extrapolating this data of depth and density of deposits along with a site plan suggested the presence

Table 7. Descriptions of test-pit excavations at Mwanga G.

Year/Trench #	Dimensions in plan	Archaeological deposit	Deposit thickness (cm)	Slag finds (kg)	Tuyère finds (kg)	Other finds
2011/A	2 m × 2 m	Dark ashy soil	10	145	35	None
2014/1	1 m × 1 m	Loose orange-grey gravelly deposit	15	0	0	None
2014/2	1 m × 1 m	Loose orange-grey gravelly deposit	15–25	1.5	0.5	None
2014/3	1 m × 1 m	Loose mid-grey sandy silt	10–35	87	7.5	2 sherds decorated pottery
2014/4	1 m × 1 m	Mid-grey sandy silt	c. 20	27.5	6	None

Table 8. Estimations of production remains at Mwanga G.

	Lower saddle	Upper saddle	Slopes
Estimated area spread of metallurgical spread (slag/tuyère)	~700 m^2	~400 m^2	~3200 m^2
Mean deposit thickness	~20 cm	~15 cm	~5 cm
Estimated volume of deposits	~105 m^3	~80 m^3	~160 m^3
Density of slag in archaeological deposits	~250 kg/m^3	~40 kg/m^3	~20 kg/m^3
Estimated slag in each area	~26,250 kg	~3200 kg	~3200 kg
Estimated weight of charcoal needed to contribute to slag	~71,925 kg	~8768 kg	~8768 kg

of a total of almost 33 tonnes of slag at the site (Table 8); combined with the slag data, it is suggested that these smelts would have required at least 90,000 kg of charcoal to have been consumed in these smelts throughout the lifetime of the site.

Understanding this in terms of the sustainability of wood resources introduces yet more uncertainty. Tree species that are preferred for charcoal used in iron smelting and smithing technologies in the Mwanga area of Pare include *S. mellifera*, *F. albida* and *A. gummifera*, all of which are relatively fast-growing, resilient species, with the capacity to withstand pollarding. In 8 to 10 years, *F. albida* is generally able to grow over 10 m in height; 5–6 m^3 of wood is generally required to produce 420 kg of charcoal (Hines and Eckman 1993). Data on charcoal yield is only available for a faster growing acacia (*Vachellia tortilis* (Forssk.) Galasso & Banfi) – for this species, 54 tonnes of fuelwood was produced per hectare (planted at 3 × 3 m) over a twelve-year growing period (Forest Division 1984). Together, these data were used to build a crude estimate of the environmental parameters that might influence impact on tree cover in Pare in reference to iron production activity.

To accommodate the limited archaeological and environmental data, especially in light of the poor chronological resolution available for the site, the potential impact of charcoal production at Mwanga G was modelled using a range of possible data for each category in order to estimate the most extreme range of forest take off scenarios possible (Table 9). This sees charcoal demand range between c. 450 kg per year (hypothesising continuous activity at the site for 200 years), up to c. 2800 kg per year (hypothesising continuous activity at the site for 25 years).

It is very difficult given the available data to assess which scenario is most likely. The two radiocarbon dates from Mwanga G suggest a minimum period of activity of between 187 and 199 years (depending on the calibration curve used, Table 6), but given the poor stratigraphic understanding of the site it is unclear as to whether this would indicate periodic or continuous activity. In terms of the regrowth and harvest capacity of *V. tortilis*, estimates of the maximum yield of fuel from a highly-managed landscape would provide c. 4000 kg of charcoal per year per hectare. A more conservative estimate would see the comfortable provision of c. 1000 kg of charcoal per year per hectare. Two hectares of land (200 m by 100 m) could thus have supported continuous production over the course of 50 years; however, if the site was active over a much more compressed timescale, the surface area that past smelters exploited would had to have been expanded. Considering the separation between clusters of smelting activity at the Mwanga sites (Figure 1), even if it is assumed that all were operating concurrently, it is feasible that smelters had access to over 10 hectares – much in excess of that required to fuel production activity over even the shortest timeframe.

4. Conclusion

This broad-brush exploration of metallurgical fuel use has served to highlight just how difficult it is to reconstruct fuel demands on environmental systems. Many factors have remained unaccounted for which would

Table 9. Modelled estimates of fuel demand at Mwanga G in light of estimates of chronological span [*ethnographic estimates provided for comparison, based on charcoal to slag ratios of 4:1 (Goucher 1981) or 3:1 (Groenewoudt and van Nie 1995)].

Years of site operation:	12.5 years	25 years	50 years	100 years	200 years
Slag produced per year	2800 kg	1400 kg	700 kg	350 kg	175 kg
Yearly charcoal demand: calculated	~7200–7600 kg	~3600–3800 kg	~1800–1900 kg	~900–950 kg	~450–480 kg
Yearly charcoal demand: ethnographic estimates*	~8400–11200 kg	~4200–5600 kg	~2100–2800 kg	~1050–1400 kg	~525–700 kg
Maximum fuelwood capacity per year (per hectare)		~4000 kg	~4000 kg	~4000 kg	~4000 kg

have served either to under- or over-estimate the impact of this production industry on woodland resources. In terms of an understanding of environmental data, this includes a lack of data on the specific regrowth rates for exploited trees, a lack of an anthracological identification of the specific tree species used in past iron smelts, and a limited understanding of the management strategies of local woodlands, such as species selection. Archaeological factors unaccounted for include that this is an assessment of data from individual sites rather than a thorough regional approach to building a holistic picture of fuel demands, integrated with an analysis of non-metallurgical fuel use. It is also difficult to estimate how many archaeological sites have been lost to or covered by erosion in this montane landscape, which would lead to an underestimation of past activity.

However, within the framework of data that are available, this study suggests that iron production was most likely not a major contributor to deforestation and erosion processes, assuming that iron production activity occurred at Mwanga G over a period of 50 years or more. The wider archaeology of the Pare area supports this hypothesis. Smithing hearths and smelting furnaces excavated in North Pare were found to have been dug into already heavily eroded land surfaces, suggesting that significant erosion processes pre-dated furnace construction and were not directly, or solely, due to reductions in slope tree cover (Iles et al. 2018). It is also clear that the iron smelting industry persisted into the nineteenth and twentieth centuries, a period for which historical records describe a high volume of iron production activity (Kersten 1869; Baumann 1891; Meyer 1891; Kotz 1922). The natural (and cultural) resources required to support a flourishing iron production industry were clearly in relatively rich supply at this time. This evidence appears therefore to support a narrative by which iron production did not play a primary role in Pare's deforestation (see Iles et al. 2018).

This raises further questions, prompting an alternative explanation for the demise of iron production in North Pare, and particularly the variety of reasons that may have led to the end of production at certain sites. One explanatory factor might relate to changes in rainfall patterns and thus river flow, which would have implications for ore availability and processing. A more important factor, however, is likely to have been prompted by the construction of the Kilimanjaro to Dar es Salaam railway in the early twentieth century, and the increase in availability of scrap iron which accompanied that new transportation (Iles et al. 2018). Other socio-environmental changes brought in during the colonial period, including changes to forestry practices and mining regulations, would also have had an impact on local iron production practices. As such, there are significant socio-economic factors that contributed to a reduction in iron production from the nineteenth century onwards. This may have been supported by a shift in rainfall patterns and climate variability (McWilliam and Packer 1999; Thomas and Nigam 2018), which may have led to diminished returns from iron production due to an increased workload to obtain and process river-sorted ore sands.

The original aim of this study was to develop a method by which to quantify the fuel ash consumption from remains of iron production commonly available on archaeological sites (i.e. slag), thus expanding opportunities to refine our understanding of the relationship between fuel consumption in iron smelting technologies and tree cover reduction. However, there are many problems that have hindered the realisation of this aim. Even when the identification of an ore body used in the past is relatively secure, it can still be difficult to obtain a sample of an ore compositionally close to that which may have been used in the past. Furthermore, if an ore contained gangue minerals geologically similar to clay contributions, it will be problematic to distinguish those components from an analysis of slag chemistry. Finally, this study has not been able to address many of the broader archaeological and environmental problems that go hand-in-hand with an estimation of the impact of charcoal use, which would have required a more refined chronological resolution and a thorough exploration of the carrying capacity of local woodlands for fuel. Despite this, this study has been able to make a broad approximation of past fuel use at the smelting site of Mwanga G and in the North Pare area more generally, taking into account the specific resource contributions to those smelting systems. It has also served to signpost the way for more exhaustive future studies of fuel use in metallurgical practices.

Acknowledgements

The author would like to acknowledge support from the British Institute in Eastern Africa (BIEA), the University of York and the University of Arizona, including the valuable mentorship of Paul Lane and David Killick, and to thank all project participants who contributed in the field, in particular Ahadi Msuya and his family. This article is based on a paper presented at the 2018 International Symposium of Archaeometry in Mérida, Mexico; the author's participation and the subsequent additional research and writing was funded by a Leverhulme Trust Early Career Fellowship held by the author at the University of Sheffield. I am grateful to Matthias Heckmann and Gail Heath for Figures 1 and 13, and for the insightful comments of an anonymous reviewer. The contents reflect only the author's views and not the views of the European Commission.

Disclosure statement

No potential conflict of interest was reported by the author.

Funding

This work was supported by a Leverhulme Trust Early Career Fellowship (ECF-2015-439) and a FP7 People: Marie-Curie Actions International Outgoing Fellowship (FP7-IOF-2012-331419).

Notes on contributor

Louise Iles holds a BSc, MSc and PhD in Archaeology from University College London. Currently, she is a Leverhulme Early Career Fellow at the Department of Archaeology, University of Sheffield. Her work examines the technological development and environmental impacts of iron production technologies across sub-Saharan Africa, blending archaeological, anthropological and archaeometallurgical methods to explore the interactions between metallurgy, environment and culture.

ORCID

Louise Iles http://orcid.org/0000-0003-4113-5844

References

Bagnall, P. 1960. "The Geology of the North Pare Mountains." *Records Geological Survey Tanganyika* 10: 7–16.

Baumann, O. 1891. *Usambara und seine Nachbargebiete*. Berlin: Dietrich Reimer.

Bronk Ramsey, C. 2009. "Bayesian Analysis of Radiocarbon Dates." *Radiocarbon* 51: 337–360.

Charlton, M., and J. Humphris. 2017. "Exploring Ironmaking Practices at Meroe, Sudan — A Comparative Analysis of Archaeological and Experimental Data." *Archaeological and Anthropological Sciences* 11: 895–912.

Crew, P. 2000. The influence of clay and charcoal ash on bloomery slags. In Il Ferro Nelle Alpi, *Proceedings of an International Conference* at Bienno, edited by C. Cucini-Tizzoni and M. Tizzoni, October 1998, 38–48.

Crew, P. 2013. "Twenty-five Years of Bloomery Experiments: Perspectives and Prospects." In *Accidental and Experimental Archaeometallurgy*, edited by D. Dungworth, and R. Doonan, 25–50. London: Historical Metallurgy Society.

David, N., R. Heinmann, D. Killick, and M. Wayman. 1989. "Between Bloomery and Blast Furnace: Mafa Iron Smelting Technology in North Cameroon." *African Archaeological Review* 7: 183–208.

Finch, J., R. Marchant, and C. Courtney-Mustaphi. 2017. "Ecosystem Change in the South Pare Mountain Bloc." *Eastern Arc Mountains of Tanzania. The Holocene* 27: 796–810.

Food and Agriculture Organization of the United Nations (FAO). 1983. *Wood Fuel Surveys. Forestry for Local Community Development Programme*. Rome: Food and Agriculture Organization of the United Nations.

Forest Division, Tanzania Ministry of Lands, Natural Resources and Tourism. 1984. *Trees for Village Forestry*. Dar es Salaam: The Ministry.

Goucher, C. 1981. "Iron is Iron 'til it is Rust: Trade and Ecology in the Decline of West African Iron-Smelting." *The Journal of African History* 22: 179–189.

Groenewoudt, B., and M. van Nie. 1995. "Assessing the Scale and Organization of Germanic Iron Production in Heeten, the Netherlands." *Journal of European Archaeology* 3: 187–215.

Haaland, R. 1985. "Iron Production, its Socio-Cultural Context and Ecological Implications." In *African Iron Working: Ancient and Traditional*, edited by R. Haaland, and P. Shinnie, 50–72. Oslo: Norwegian University Press.

Håkansson, N. 2008. "The Decentralized Landscape: Regional Wealth and the Expansion of Production in Northern Tanzania Before the eve of Colonialism." In *Economies and the Transformation of Landscape*, edited by L. Cliggett, and C. Pool, 239–265. Lanham: Alta Mira Press.

Heath, G. 2015. *Magnetic Results of Iron Smelting Activities in East Africa*. Unpublished Report on Behalf of EnvIron Project. Tucson: University of Arizona.

Heckmann, M. 2011. *Soil erosion history and past human land use in the North Pare Mountains. A geoarchaeological study of slope deposits in NE Tanzania*. University of York, UK. Unpublished PhD thesis.

Hines, D., and K. Eckman. 1993. *Indigenous Multipurpose Trees of Tanzania: uses and economic benefits for people*. Food and Agriculture Organization of the United Nations, Rome.

Hogg, A., Q. Hua, P. Blackwell, M. Niu, C. Buck, T. Guilderson, T. Heaton, et al. 2013. "SHCal13 Southern Hemisphere Calibration, 0-50, 000 Years cal BP." *Radiocarbon* 55: 1889–1903.

Holy, L. 1957. Získávání a zpracovávání železa u východoafrických Bantu. *Československá Ethnografie* 5: 273–288, 348–367.

Humphris, J. 2010. "An Archaeometallurgical Investigation of Iron Smelting Traditions in Southern Rwanda." Unpublished PhD thesis, UCL, London.

Ige, A. 2013. "Yoruba Iron Metallurgy: raw Materials, Routine and Rituals." In *The World of Iron*, edited by J. Humphris, and T. Rehren, 29–34. London: Archetype.

Ige, A., and T. Rehren. 2003. "Black Sand and Iron Stone: Iron Smelting in Modakeke, Ife, South Western Nigeria." *IAMS* 22: 19–21.

Iles, L. 2016. "The Role of Metallurgy in Transforming Global Forests." *Journal of Archaeological Method and Theory* 23: 1219–1241.

Iles, L., and M. Martinón-Torres. 2009. "Pastoralist Iron Production on the Laikipia Plateau, Kenya: Wider Implications for Archaeometallurgical Studies." *Journal of Archaeological Science* 36: 2314–2326.

Iles, L., D. Stump, M. Heckmann, C. Lang, and P. Lane. 2018. "Iron Production in North Pare, Tanzania: Archaeometallurgical and Geoarchaeological Perspectives on Landscape Change." *African Archaeological Review* 35: 507–530.

Itaya, H., T. Watanabe, M. Hayashi, and K. Nagata. 2014. "Phase Diagram of FeO-TiO_2-SiO_2-5%Al_2O_3 Slag (Phase Diagram of Smelting Slag of Titanium Oxide Bearing Iron Sand)." *ISIJ International* 54: 1067–1073.

Jackson, C., C. Booth, and J. Smedley. 2005. "Glass by Design? Raw Materials, Recipes and Compositional Data." *Archaeometry* 47: 781–795.

Kersten, O. 1869. *Baron Carl Claus von der Decken's reisen in Ost-Afrika in den jahren 1862 bis 1865*. Vol. II. Graz: Akademische Druck und Verlagsanstalt.

Killick, D., and D. Miller. 2014. "Smelting of Magnetite and Magnetite-Ilmenite Iron Ores in the Northern Lowveld, South Africa, ca. 1000 CE to ca. 1880 CE." *Journal of Archaeological Science* 43: 239–255.

Kimambo, I. 1996. "Environmental Control and Hunger in the Mountains and Plains of Northern Tanzania." In

Custodians of the Land: Ecology and Culture in the History of Tanzania, edited by G. Maddox, J. Giblin, and I. Kimambo, 71–95. London: James Currey.

Kotz, E. 1922. *Im Banne der Furcht: Sitten und Gebräuche der Wapare in Ostafrika*. Advent-Verlag: Hamburg.

Lyaya, E. 2013. "Use of Charcoal Species for Ironworking in Tanzania." In *The World of Iron*, edited by J. Humphris, and T. Rehren, 444–453. London: Archetype.

Mapunda, B. 2003. *Iron Technology and Deforestation: Myths and Realities*. AFRAS: University of Sussex.

Mbaga-Semgalawe, Z., and H. Folmer. 2000. "Household Adoption Behaviour of Soil Conservation: the Case of North Pare and West Usambara Mountains of Tanzania." *Land Use Policy* 17: 321–336.

McWilliam, N., and M. Packer. 1999. " Climate of Mkomazi: Variability and Importance." In *Mkomazi: The Ecology, Biodiversity and Conservation of a Tanzanian Savanna*, edited by M. Coe, N. McWilliam, G. Stone, and M. Packer, 15–24. London: Royal Geographical Society (with The Institute of British Geographers).

Meyer, H. 1891. *Across East African Glaciers: an Account of the First Ascent of Kilimanjaro* [translated by E. Calder]. London: George Philip & Son.

Mwampamba, T., A. Ghilardi, K. Sander, and K. Chaix. 2013. "Dispelling Common Misconceptions to Improve Attitudes and Policy Outlook on Charcoal in Developing Countries." *Energy for Sustainable Development* 17: 75–85.

Paynter, S., P. Crew, E. Blakelock, and G. Hatton. 2015. "Spinel-rich Slag and Slag Inclusions from a Bloomery Smelting and Smithing Experiment with Sideritic Ore." *Historical Metallurgy* 49: 126–143.

Pleiner, R. 2000. *Iron in Archaeology. The European Bloomery Smelters*. Archeologicky Ústav Avcr: Praha.

Reimer, P., E. Bard, A. Bayliss, J. Beck, P. Blackwell, C. Bronk Ramsey, P. Grootes, et al. 2013. "IntCal13 and Marine13 Radiocarbon age Calibration Curves 0–50,000 Years cal BP." *Radiocarbon* 55: 1869–1887.

Rostoker, W., and B. Bronson. 1990. *Pre-Industrial Iron: its Technology and Ethnology*. Philadelphia: Pennsylvania University Press.

Schmidt, P. 1989. "Early Exploitation and Settlement in the Usambara Mountains." In *Forest Conservation in the East Usambara Mountains, Tanzania*, edited by A. Hamilton, and R. Bensted-Smith, 75–78. Gland: IUCN.

Serneels, V., and P. Crew. 1997. "Ore-slag Relationships from Experimentally Smelted bog-Iron ore." In *Early Ironworking in Europe: Archaeology and Experiment*, edited by P. Crew, and S. Crew, 78–82. Maentwrog: Plas Tan y Bwlch.

Sheridan, M. 2001. "Cooling the Land: the political ecology of the North Pare Mountains, Tanzania." Unpublished Ph.D. thesis, Harvard University, Cambridge.

Stump, D. 2010. "Ancient and Backward or Long-Lived and Sustainable?" The Role of the Past in Debates Concerning Rural Livelihoods and Resource Conservation in Eastern Africa." *World Development* 38: 1251–1262.

Thomas, N., and S. Nigam. 2018. "Twentieth-Century Climate Change Over Africa: Seasonal Hydroclimate Trends and Sahara Desert Expansion." *Journal of Climate* 31: 3349–3370.

van der Merwe, N., and D. Avery. 1987. "Science and Magic in African Technology: Traditional Iron Smelting in Malawi." *Africa* 57: 143–172.

Verein Deutscher Eisenhüttenleute. 1995. *Slag Atlas*. Verlag Stahleisen Gmbtt: Düsseldorf.

Yao, Z., M. Xia, H. Li, T. Chen, Y. Ye, and H. Zheng. 2014. "Bivalve Shell: not an Abundant Useless Waste but a Functional and Versatile Biomaterial." *Critical Reviews in Environmental Science and Technology* 44: 2502–2530.

Ylhäisi, J. 2004. "Indigenous Forests Fragmentation and the Significance of Ethnic Forests for Conservation in the North Pare, the Eastern Arc Mountains, Tanzania." *Fennia* 182: 109–132.